REFLECTANCE CORRECTION FOR PERSPIRING FACES

W.A.P. Smith, A. Robles-Kelly, E.R. Hancock

Department of Computer Science, The University of York, York, YO1 5DD, UK
{wsmith, arobkell, erh}@cs.york.ac.uk

ABSTRACT

We present a parameter-free method for estimating the BRDF of a subject's skin from a single image. We show how the technique can be used to remove specularities caused by perspiration or oil on the skin's surface and demonstrate that this yields improved analysis using shape from shading.

1. INTRODUCTION

Variation in images of faces can be conceptually divided into a number of subspaces, which are chosen to reflect useful facial dimensions. Commonly these subspaces are: identity, expression, pose and lighting. A further and often neglected source of variation is due to the reflectance properties of skin, which can cause dramatic differences in the appearance of a face. Variation in skin reflectance can be attributed primarily to three factors: melanin concentration, haemoglobin concentration and the amount of perspiration or oil present at the skin's surface. All three factors can vary for a given subject due to exposure to U.V. radiation and variation in body temperature, but it is the specularities caused by perspiration or oil that are responsible for the biggest variation in a face's appearance.

For this reason, the accurate modelling of skin reflectance is of considerable topicality in machine face recognition. The bi-directional reflectance distribution function (BRDF) of a subject's skin may itself contain useful biometric information, thus providing features for face recognition and classification. It may also provide information about the condition of the skin such as the presence of abnormalities. Moreover, many techniques proposed for face recognition rely on the assumption that skin is a perfect Lambertian reflector [1, 2, 3]. If an accurate BRDF is to hand then photometric correction may be applied to recover the Lambertian reflectance component. This correction process may prove useful for removing specularities, which is of particular importance if the images are to be analysed using shape from shading. Further, just as shape free faces have proven more suitable for recognition using principal component analysis [4], reflectance normalised faces would also be more accurately modelled in linear spaces if photometric correction is applied as a preprocessing step.

The methods used to model or approximate the BRDF can be divided into those that are physics-based, semi empirical or empirical in nature. In the case of skin, its complex physical nature has meant the majority of work has concentrated on computationally efficient models capable of realistic skin rendering. In the graphics community, it is the phenomenological sub-surface scattering model of Hanrahan and Krueger [5] that has been most widely adopted, due to its efficient implementation and visually accurate renderings. More recently, Jensen et al [6] have developed a model of subsurface light transport which has been shown to produce superior renderings to that of Hanrahan and Krueger.

However, neither the models developed in physics nor the computational models developed in graphics are well suited for skin analysis tasks in computer vision. An alternative is to make empirical estimates (or learn) the BRDF under controlled lighting and viewing conditions. The main problem with this approach is that the BRDF has four degrees of freedom, that correspond to the zenith and azimuth angles for the light source and the viewer. As a result the tabulation of empirical BRDF's can be slow and labour intensive. Moreover, since these methods require a perfectly stationary, flat sample, they are badly suited to taking measurements from skin samples of live subjects. Marschner et al have gone some way to solving these problems [7].

The fact that skin reflectance properties vary so widely both between subjects and between the same subject at different times, means that no empirically measured BRDF will suffice to characterise skin reflectance in general. Likewise, none of the limited number of reflectance models applicable to computer vision could accurately capture the wide variation in skin reflectance properties. For this reason, an empirical image based BRDF estimation technique is best suited to computer vision tasks involving skin. In the next section we present a novel parameter free method for estimating skin BRDFs from a single image under conditions in which the light source and viewer direction are identical.

2. IMAGE BASED BRDF APPROXIMATION

We simplify the problem of estimating the radiance function by exploiting differential geometry and making use of

0-7803-8554-3/04/$20.00

the Gauss map from the surface onto a unit sphere. For an orientable surface $S \in \Re^3$, the Gauss map $G : S \mapsto \hat{S}$ maps points on the surface S onto locations on the unit sphere $\hat{S}$ which have identical surface normal directions. Our aim is to use correspondences between surface normal directions to map brightness values from the image onto the unit sphere. The polar distribution of brightness on the unit sphere $\hat{S}$ is the radiance function for the surface.

Provided that the reflectance properties of the surface are isotropic and homogeneous then the problem is simplified considerably if the viewer and light source directions are identical. The isotropy assumption will ensure that circles of latitude on the unit sphere will have constant brightness. The problem of recovering the distribution of brightness with latitude becomes that of estimating the zenith angle from the distribution of image brightness.

Hence, we specialise our discussion to the case where the plane Π is chosen so that the viewer direction vector $\vec{\mathbf{V}}$ and the light-source direction vector $\vec{\mathbf{L}}$ are co-incident, i.e. $\vec{\mathbf{L}} = \vec{\mathbf{V}}$. Suppose that the point p on the unit sphere has zenith angle θ_p and azimuth angle α_p. Under the Gauss map, the brightness value associated with this point is denoted by the polar radiance function $f_O(\theta_p, \alpha_p) = I_s$, where I_s is the measured brightness at the corresponding point s in the image of the surface S. As noted above, when the viewer and light source directions are identical, then provided that the reflectance process is isotropic, then the distribution of radiance across the unit sphere can be represented by a function $g(\theta_p)$ of the zenith angle alone. As a result, the observed brightness values mapped onto the unit sphere by the Gauss map G can be generated by revolving the function $g(\theta_p) = f_O(\theta_p, 0)$ in azimuth angle α_p about the axis defined by the viewer and light source directions. The problem of describing the observed brightness distribution over the Gauss sphere hence reduces to that of approximating the function $g(\theta_p)$ and computing its trace of revolution.

The Cartesian image of the unit sphere under orthographic projection onto the plane $\hat{\Pi}$ can hence be represented using polar-coordinates as:

$$I_{\hat{\Pi}}(\sin\theta_p \cos\alpha_p, \sin\theta_p \sin\alpha_p) = f_O(\theta_p, \alpha_p) \qquad (1)$$

In fact, when the light source and viewer directions are identical, then the image is circularly symmetric and we can write

$$I_{\hat{\Pi}}(\sin\theta_p \cos\alpha_p, \sin\theta_p \sin\alpha_p) = g(\theta_p) \qquad (2)$$

It is possible to estimate $g(\theta_p)$ using the differential structure of the observed brightness on the image plane Π. $g(\theta_p)$ can be rewritten as the integral of the partial derivative of the observed brightness with respect to the angular variable θ_p. As a result, $g(\theta_p)$ is given by

$$g(\theta_p) = \frac{1}{2\pi} \int_0^{2\pi} \int_0^{\theta_p} \frac{\partial f_O(\theta, \alpha)}{\partial \theta} d\theta d\alpha \qquad (3)$$

In other words, the generating function $g(.)$ on the unit sphere can be expressed in term of the cumulative distribution of the derivatives of the radiance function or alternatively the derivatives of the image brightness.

We now turn our attention to the image of the unit sphere on the plane $\hat{\Pi}$. Suppose that $F(r_p, \theta_p)$ is a parametric polar function that represents the distribution of radiance over the image of the unit sphere. The radial component of this function can be used to approximate the generator of the radiance function on the unit sphere $\hat{S}$, i.e. $g(\theta_p)$. The radial co-ordinate of the function is the Euclidean distance between the point p and the center-point of the unit sphere $\hat{S}$ on the viewer plane $\hat{\Pi}$, i.e. $r_p = \sqrt{(\sin\theta_p \cos\alpha_p)^2 + (\sin\theta_p \sin\alpha_p)^2} = \sin\theta_p$. Hence

$$F(r_p, \theta_p) = \begin{bmatrix} r_p \\ g(\theta_p) \end{bmatrix} = \begin{bmatrix} \sin\theta_p \\ \frac{1}{2\pi} \int_0^{2\pi} \int_0^{\theta_p} \frac{\partial f_O(\theta,\alpha)}{\partial \theta} d\theta d\alpha \end{bmatrix} \qquad (4)$$

Since the surface normals are not to hand, the correspondences between locations on the surface and the unit sphere are not available. Hence, the quantity θ_p is unknown. In other words, the function $F(r_p, \theta_p)$ only allows the surface S to be mapped onto the unit sphere $\hat{S}$ in an implicit manner.

This lack of correspondence information can be overcome by using the distribution of brightness gradients on the image plane to estimate the radiance function. To do this, we commence by showing the relation between the image brightness gradient $\mid \nabla I_s \mid$ and the function $g(\theta_p)$. Since the image is circularly symmetric, the image gradient can be rotated about the z-axis without any loss of generality. We align the image gradient with the azimuth direction using the rotation matrix

$$R_z = \begin{bmatrix} \cos(\alpha_p) & \sin(\alpha_p) \\ -\sin(\alpha_p) & \cos(\alpha_p) \end{bmatrix} \qquad (5)$$

which rotates the vector ∇I_s by an angle α_p in a clockwise direction about the z-axis.

The image brightness derivatives may be related to those of the function $g(\theta_p)$ using the inverse Jacobian via the following matrix equation

$$R_z \begin{bmatrix} \frac{\partial I_s}{\partial x} \\ \frac{\partial I_s}{\partial y} \end{bmatrix} = J^{-1} \begin{bmatrix} \frac{\partial g(\theta_p)}{\partial \theta_p} \\ \frac{\partial g(\theta_p)}{\partial \alpha_p} \end{bmatrix} \qquad (6)$$

where the Jacobian matrix for the transformation from the image to the unit sphere is

$$J = \begin{bmatrix} \frac{\partial x}{\partial \theta_p} & \frac{\partial x}{\partial \alpha_p} \\ \frac{\partial y}{\partial \theta_p} & \frac{\partial y}{\partial \alpha_p} \end{bmatrix} = \begin{bmatrix} \frac{\partial(\sin(\theta_p)\cos(\alpha_p))}{\partial(\theta_p)} & \frac{\partial(\sin(\theta_p)\cos(\alpha_p))}{\partial(\alpha_p)} \\ \frac{\partial(\sin(\theta_p)\sin(\alpha_p))}{\partial(\theta_p)} & \frac{\partial(\sin(\theta_p)\sin(\alpha_p))}{\partial(\alpha_p)} \end{bmatrix} \qquad (7)$$

Using the rotation on the image plane and the coordinate transformation between the image plane and the unit sphere,

we find that

$$|\nabla I_s| = \frac{1}{\cos\theta_p}\frac{\partial g(\theta_p)}{\partial \theta_p} = \frac{\partial g(\theta_p)}{\partial \sin\theta_p} \quad (8)$$

In this way, we can relate the image gradient to the derivative of the function $g(\theta_p)$ with respect to the zenith angle θ_p. In terms of finite differences, the relationship between the image gradient and the changes $\Delta g(\theta_p)$ in $g(\theta_p)$ and $\Delta \sin\theta_p$ in θ_p is the gradient of the function $F(r_p, \theta_p)$, i.e. $|\nabla I_s| = \frac{\Delta g(\theta_p)}{\Delta \sin\theta_p}$. Furthermore, on the unit sphere $\hat{S}$, it is always possible to choose points to be sampled so that the difference in brightness is a constant τ. As a result, we can write $\Delta \sin\theta_p = \frac{\tau}{|\nabla I_s|}$.

To recover θ_p from the expression above we perform numerical integration. To do this we sort the image gradients according to the associated image brightness values. Accordingly, let $\mid \nabla I \mid_l$ be the image gradient associated with the brightness value l. The numerical estimate of $\sin\theta_p$ is found by summing or integrating the distribution of gradients over brightness

$$\sin\theta_p = \sum_{l=1}^{m} \frac{\tau}{\mid \nabla I_s \mid_l} + \kappa \quad (9)$$

where κ is the integration constant and m is the maximum brightness value. Hence, we can use the cumulative distribution of inverse gradients to index the zenith angle on the unit sphere. This indexation property means that we can approximate the function $F(r_p, \theta_p)$ or equivalently $g(\theta_p)$ by tabulation.

To pursue this idea, in principle, we only require a single image gradient corresponding to each of the distinct brightness levels in the image. In practice, we make use of the cumulative distribution of image gradients in order to minimise the approximation error by averaging. Let $H(l) = \{s \mid I_s = l\}$ be the set of pixels with brightness value l. For the brightness value $l = g(\theta_p)$, the average gradient is given by

$$h(l) = \frac{\sum_{(s)\in H(l)} \mid \nabla I_s \mid}{\mid H(l) \mid} \quad (10)$$

The distribution of average gradient over brightness is stored as a vector h. Zero entries of the vector, which correspond to brightness values that are not sampled in the image, can cause divide-by-zero errors when the radiance function is computed. To overcome this problem, we smooth the components of the vector by performing piecewise linear interpolation of the adjacent non-zero elements. The resulting vector is denoted by $\hat{h}$ With the average image gradient to hand, we define the tabular approximation $\hat{F}$ to $F(r_p, \theta_p)$ as the set of Cartesian pairs

$$\hat{F} = \{((\tau \sum_{i=1}^{l} \hat{h}(l)^{-1} + \kappa), l); l = 1, 2, \ldots, n_{max}\} \quad (11)$$

where n_{max} is the maximum brightness value in the image. All that remains is to compute the constants τ and κ. We do this by making use of the maximum and minimum values of $\sin\theta_p$. Since the maximum and minimum values of $\sin\theta_p$ are unity and zero when $\theta_p = \frac{\pi}{2}$ and $\theta_p = 0$, we can set κ to unity. Evaluating the numerical integral for $l = n_{max}$ (i. e. $\sin 0 = 0$), we get $\tau = -\sum_{i=1}^{n_{max}} \hat{h}(i)^{-1}$.

3. EXPERIMENTS

In this section we provide some experimental results obtained by applying the BRDF approximation technique described in the previous section to images of faces. We commence by demonstrating the effect of increased specular reflection on the recovered reflectance estimate. Next, we focus on photometric correction by re-rendering the images using Lambert's law to remove specularities. Finally, we show needle maps and curvedness estimates recovered from the images using shape from shading before and after the application of photometric correction.

In all images the subjects were illuminated by a single light source situated close to the viewer. Figure 1 shows three images of the same subject along with their corresponding estimated reflectance function, $\hat{F}$ as a function of $\sin\theta_p$. Perfect Lambertian reflectance is shown by the broken line. From left to right they have increasing amounts of artificial perspiration applied, simulated by spraying a water-based solution onto the skin. The increased specular reflection is clearly evident in the estimated reflectance functions, with the specular spike where $\sin\theta_p \simeq 0$ becoming more pronounced as the perspiration increases.

The first two rows of figure 2 show the effect of Lambertian re-mapping on three images of perspiring faces. The top row shows the original images. The second row shows the faces after exchanging the estimated reflectance function with Lambert's law. The strong specularities have been cleanly removed and the intensity gradients across the three faces have been enhanced. These images would clearly be more suitable for shape-from-shading analysis than the originals.

The third and fourth rows show the needle maps recovered using shape from shading before and after Lambertian re-mapping. The surface detail is clearer in the needle maps recovered after Lambertian re-mapping and the noise around areas of specular reflection has been removed. Finally, the fifth and sixth rows show the curvedness estimated from the surface normals. Specularities cause erroneous areas of high curvedness. It is clear from the curvedness plots that the Lambertian re-mapping has successfully corrected these whilst still maintaining the surface structure around the nose.

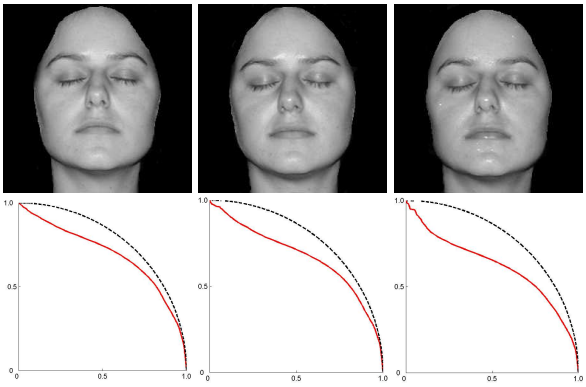

Fig. 1. Estimated reflectance functions for increasing amounts of perspiration

4. CONCLUSIONS

In this paper we have described a parameter free method for estimating the BRDF for human skin. The method has been successfully applied to remove facial specularities caused by perspiration or oily skin. In addition, these reflectance corrected images have been demonstrated to yield improved needle maps and curvedness estimates. There are a number of ways in which the work described in this paper can be further developed. First, the corrected Lambertian images can be used for the purposes of face shape analysis and recognition. Second, the acquired reflectance models can be used for face synthesis and may find applications in biometric identification or identifit modelling.

5. REFERENCES

[1] P. N. Belhumeur, J. Hespanha, and D. J. Kriegman, "Eigenfaces vs. fisherfaces: Recognition using class specific linear projection," *IEEE Trans. PAMI*, vol. 17, no. 7, pp. 711–720, 1997.

[2] A. Georghiades, D. Kriegman, and P. Belhumeur, "Illumination cones for recognition under variable lighting: Faces," in *IEEE Conf. CVPR*, 1998, pp. 52–59.

[3] W. A. P. Smith and E. R. Hancock, "Face recognition using shape-from-shading," in *13th British Machine Vision Conference*, 2002, vol. 2, pp. 597–606.

[4] I. Craw and P. Cameron, "Parameterising images for recognition and reconstruction," in *2nd British Machine Vision Conference*, 1991, pp. 367–370.

[5] P. Hanrahan and W. Krueger, "Reflection from layered surfaces due to subsurface scattering," in *Proceedings of the 20th annual conference on Computer graphics and interactive techniques*, 1993, pp. 165–174.

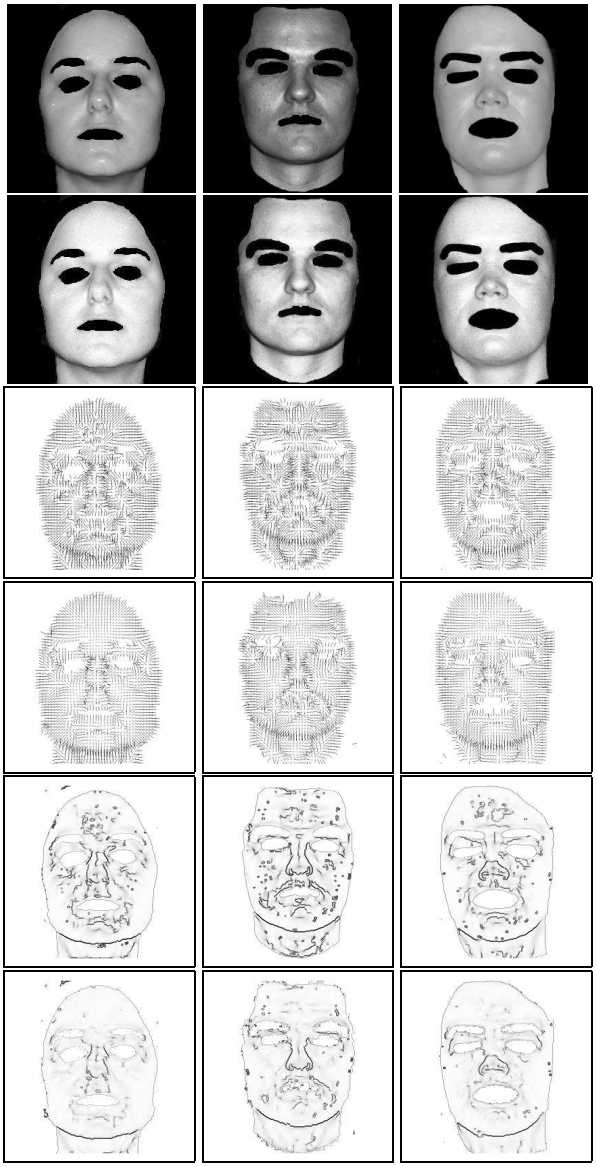

Fig. 2. Needle maps and curvedness estimates before and after photometric correction

[6] H.W. Jensen, S.R. Marschner, M. Levoy, and P. Hanrahan, "A practical model for subsurface light transport," in *Proceedings of SIGGRAPH 2001*, August 2001, pp. 511–518.

[7] S.R. Marschner, S.H. Westin, E.P.F. Lafortune, K.E. Torrance, and D.P. Greenberg, "Reflectance measurements of human skin," Tech. Rep. PCG-99-2, Program of Computer Graphics, Cornell University, 1999.